Supporting Information

Ultrafast degradation of organic pollutants enabled by nanofluidic

ZIF-67/GO membranes via efficient nanoconfined

peroxymonosulfate activation

Jian Hu, [a] Jue Hou, [a] Chen Zhao, [a] Yuyu Su, [a] Rong Wang, [b] and Huacheng Zhang *[a]

a Chemical and Environmental Engineering, School of Engineering, RMIT University, Melbourne, VIC 3000, Australia

E-mail: huacheng.zhang@rmit.edu.au

b School of Civil and Environmental Engineering, Nanyang Technological University, 50 Nanyang Avenue, 639798, Singapore

Experimental Procedures

Chemical and materials

Cobalt (II) nitrate hexahydrate ($Co(NO_3)_2 \cdot 6H_2O$), 2-methylimidazole (Hmim), triethylamine (TEA), bisphenol A, potassium peroxymonosulfate (PMS, $KHSO_5 \cdot 0.5KHSO_4 \cdot 0.5K_2SO_4$), potassium sulfate ($K_2SO_4$), p-benzoquinone (BQ), tert-Butyl alcohol (TBA), L-histidine, nitro blue tetrazolium (NBT), terephthalic acid, benzoic acid, sodium sulfate, tetracycline, phenol, methylene blue, methyl orange, Congo red were purchased from Sigma-Aldrich Pty. Ltd. Methanol was purchased from Thermo Fisher Scientific, Australia. Sodium carbonate (Na_2CO_3) was purchased from Chem-Supply, Australia. Sodium hydrogen carbonate ($NaHCO_3$) was purchased from Rowe Scientific Pty Ltd, Australia.

GO preparation

The graphitic oxide was prepared by stirring 100 grams of powdered flake graphite and 50 grams of sodium nitrate into 2.3 liters of sulfuric acid. The mixture was combined in a 15-liter battery jar, which was cooled to 0°C in an ice bath for safety. While maintaining vigorous agitation, 300 grams of potassium permanganate was gradually added to the suspension, ensuring the temperature did not exceed 20°C. The ice bath was then removed, and the temperature of the suspension was brought to 35 ± 3°C, where it was maintained for 30 minutes. As the reaction progressed, the mixture gradually thickened, with a diminishing amount of effervescence. After 20 minutes, the mixture became pasty, producing only a small amount of gas. The resulting paste was brownish-grey in color.

At the end of 30 minutes, 4.6 liters of water was slowly stirred into the paste, causing violent effervescence and an increase in temperature to 98°C. The diluted suspension, now brown in color, was maintained at this temperature for 15 minutes. The suspension was then further diluted to approximately 14 liters with warm water and treated with 3% hydrogen peroxide to reduce the residual permanganate and manganese dioxide to colorless, soluble manganese sulfate. Upon treatment with the peroxide, the suspension turned bright yellow. The suspension was filtered, resulting in a yellow-brown filter cake. Filtering was conducted while the suspension was still

warm to avoid precipitation of the slightly soluble salt of mellitic acid formed as a side reaction.

After washing the yellowish-brown filter cake three times with a total of 14 liters of warm water, the graphitic oxide residue was dispersed in 32 liters of water to approximately 0.5% solids. The remaining salt impurities were removed by treating with resinous anion and cation exchangers. The dry form of graphitic oxide was obtained by centrifugation followed by dehydration at 40°C over phosphorus pentoxide in vacuo.

GO suspension

The suspension was centrifuged and dialyzed in water to wash. A GO suspension with a concentration of 5 mg/ml was obtained. The GO aqueous solution was then further diluted to 1 mg/ml with methanol (analysis, Merck) and subjected to 5 hours of sonication. The final solvent for the GO was a water-methanol mixture (1:4, v/v).

Catalytic activity of ZIF-67/GO-x membrane

All the catalytic experiments were conducted at 20°C and the pH of reaction solutions was maintained at 10.4 using the 0.001 M carbonate/hydrogen carbonate buffer system (2.1mg NaHCO$_3$ and 18.55 mg Na$_2$CO$_3$ in 200 ml Milli-Q water). In a typical experiment, 100 mL of 5 mg L^{-1} BPA buffer solution went through the ZIF-67/GO-x membrane first to reach the adsorption-desorption equilibrium. The mixed buffer solution containing BPA (5 ppm) and PMS (200 ppm) was filtered through the ZIF-67/GO-x membrane at a working pressure of 0.08 MPa. The permeate samples were collected every 20 min and analyzed using high-performance liquid chromatography (HPLC, Agilent, 1220 Infinity LC) at a detection wavelength of 230 nm with a Poroshell 120 EC-C18 column (4.6 × 150 mm, 2.7-Micron). The mobile phase comprised a methanol/water mixture (70:30, v/v).

The degradation efficiency of BPA can be calculated as follows:

$$\text{BPA degradation efficiency (\%)} = (1 - \frac{C_P}{C_F}) \times 100 \tag{1}$$

where C_P and C_F stand for the concentrations of BPA in the permeate and feed sides, respectively.

The flux of the ZIF-67/GO-x membrane was calculated as follows:

$$J = \frac{V}{S \times T}$$

(2)

where J stands for the permeate flux (L m^{-2} h^{-1}, V stands for the membrane permeate volume (L), S stands for the effective surface area of the membrane (m^2), and T stands for the experimental time (h).

For the batch suspension reaction, the same amount of ZIF-67/GO nanosheets was added into 50 mL BPA (5 ppm) buffer solution. After 30 min stirring to reach adsorption-desorption equilibrium, PMS (200 ppm) was added into the mixed solution to initiate the reaction. The sample was taken every 20 min and then was analyzed by the HPLC.

The concentration of leached cobalt ions was analyzed by the inductively coupled plasma optical emission spectrometer (ICP, 7700 Series ICP-MS, Agilent).

The BPA intermediate products during the reaction were detected by the liquid chromatography-mass spectroscopy (1260 Infinity II LC system w/ MSD) with a Poroshell 120 EC-C18 column (4.6 × 150 mm, 2.7 micron). The flow rate of the mobile phase is 0.25 mL/min, which consists of water and methanol. The Agilent MassHunter Workstation software is employed for the analysis of the reaction byproducts.
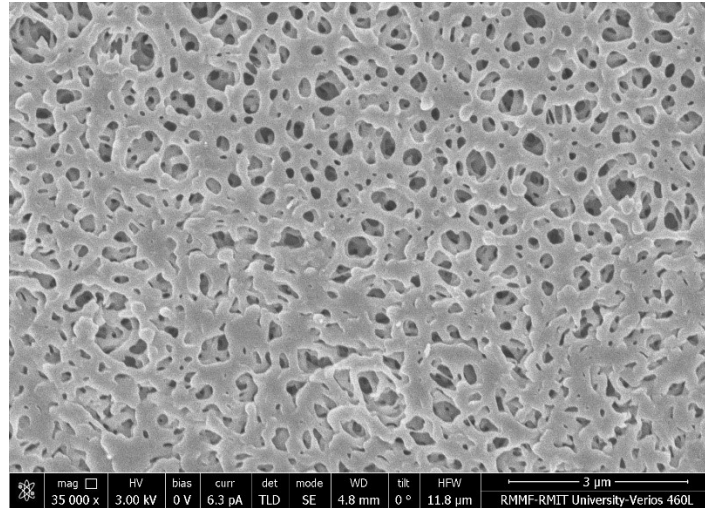
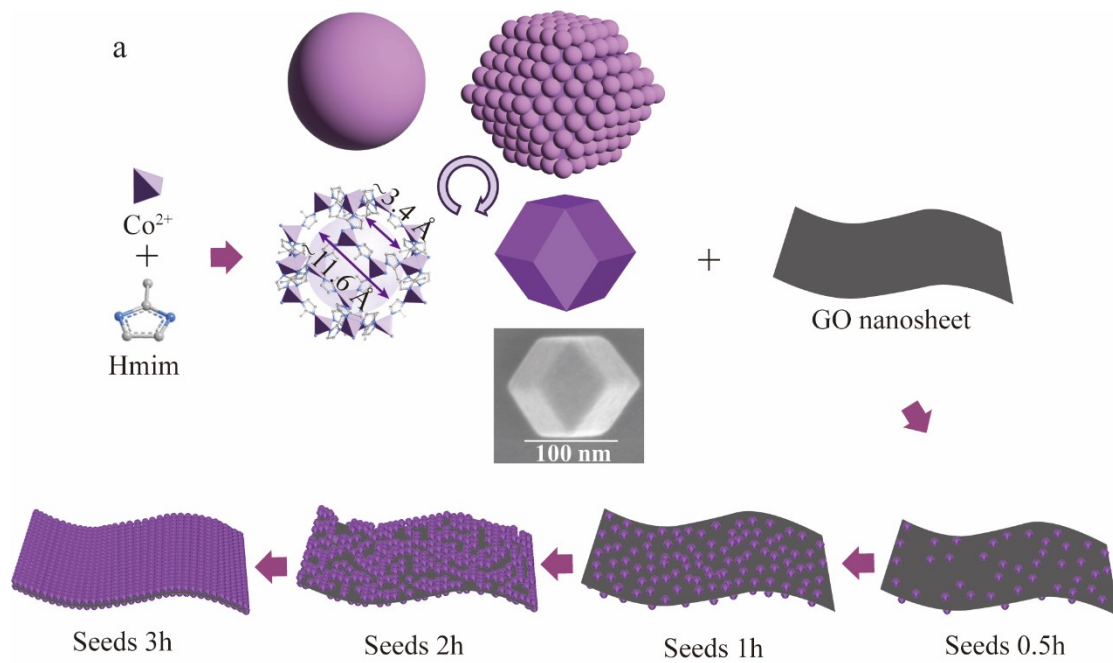**Figure S1.** SEM image of the top surface of the PES substrate.

Figure S2. Schematic illustration of the synthesis of ZIF-67/GO with different synthesis times.
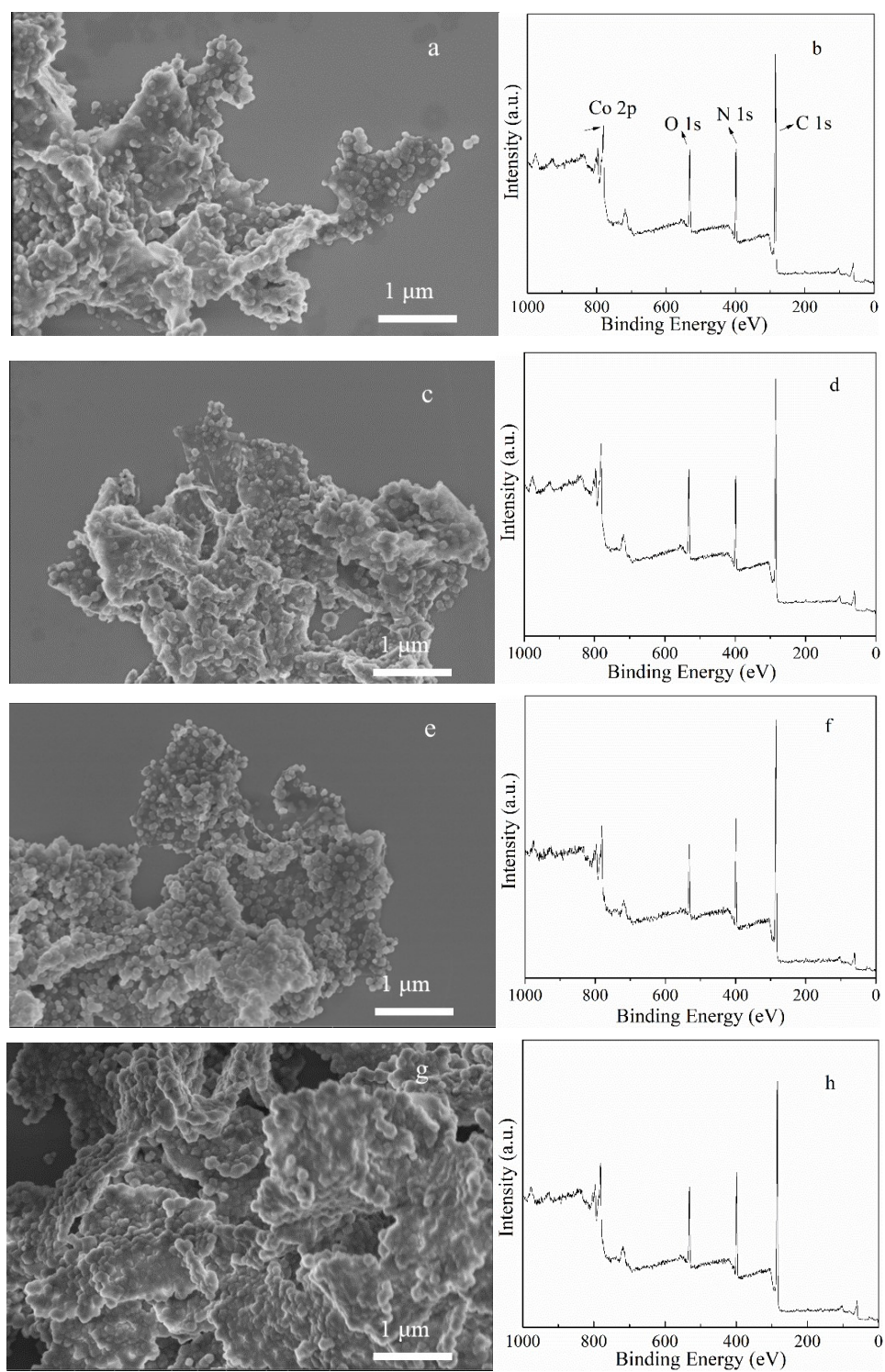
Figure S3. (a), (c), (e), (g) SEM images of ZIF-67/GO-0.5, ZIF-67/GO-1, ZIF-67/GO-2, and ZIF-67/GO-3, respectively. (b), (d), (f), (h) XPS survey spectra of ZIF-67/GO-0.5, ZIF-67/GO-1, ZIF-67/GO-2, and ZIF-67/GO-3, respectively.
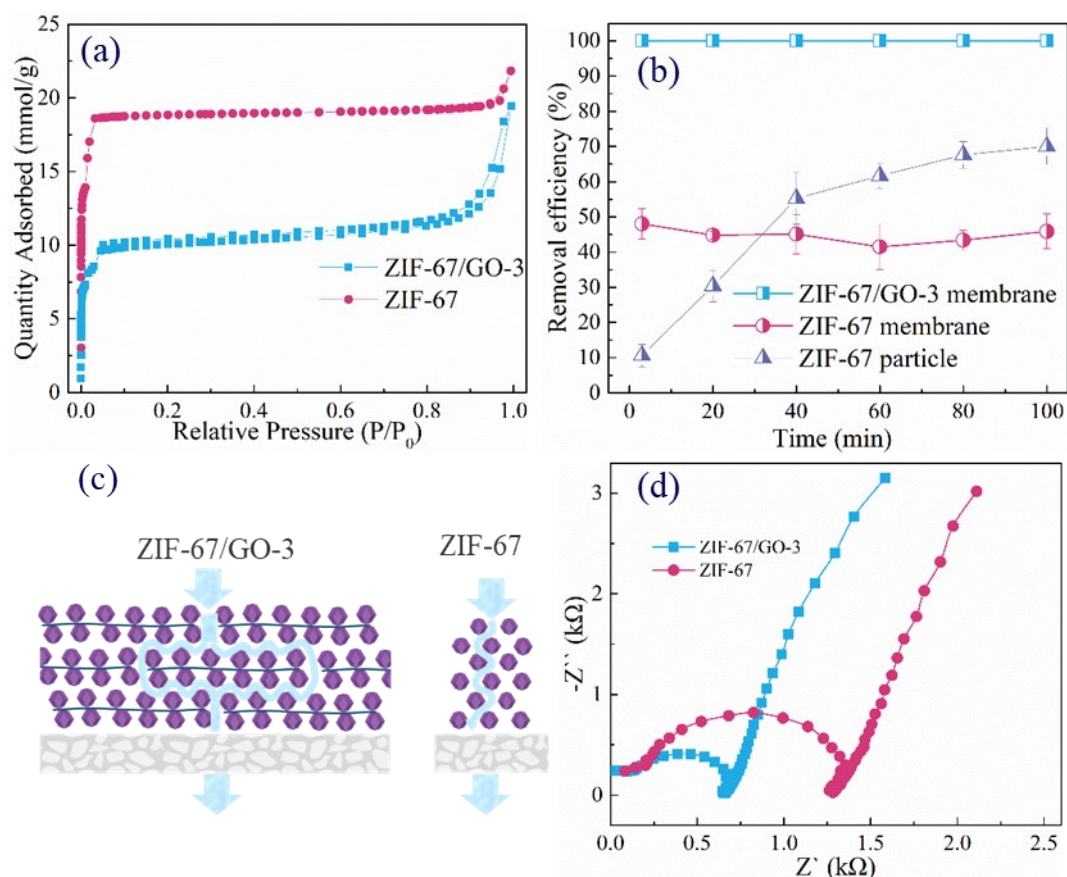
Figure S4. (a) N₂-adsorption/desorption isotherms, (b) Degradation efficiency of BPA, (c) plausible passing route of BPA molecules, and (d) Electrochemical impedance spectroscopy (EIS, Nyquist plots) at open circuit potential for ZIF-67GO-3 and ZIF-67. Reaction conditions: [BPA] = 5 mg L^{-1}, [PMS] = 200 ppm, and pH 10.4.
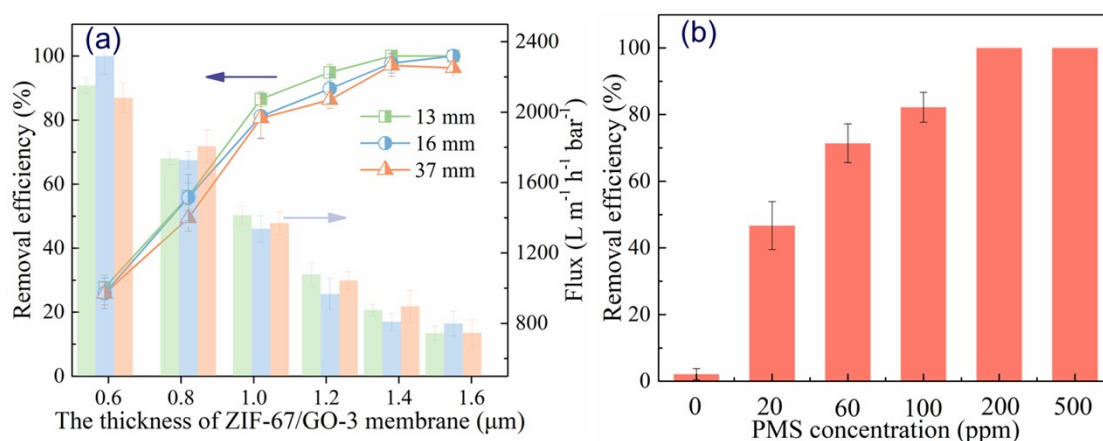

Figure S5. (a) Permeance of ZIF-67/GO-3 membrane and efficiency of BPA removal as a function of membrane thickness and area sizes of membranes. (b) Optimization of PMS concentration over ZIF-67/GO-3 membrane/PMS system towards BPA degradation.

To balance the catalytic performance and permeance, the thickness and area sizes of the ZIF-67/GO-3 membrane were optimized. Fig. S5a displayed that the catalytic performance developed,

but the water flux dropped with the increase in membrane thickness. 100% BPA degradation efficiency could be realized at a membrane thickness of $\geq$ 1.38 μm. In addition, the membrane removal efficiency and flux are similar as the membrane diameter increases from 13 to 37 mm. There seemed to be no difference in the BPA removal efficiency for different area sizes of the membrane. So, a membrane diameter of 13 mm was selected for the following studies.

For the retention time curve of Fig. 2(b), the retention time came from the different thicknesses of the ZIF-67/GO-3 membrane.

For the PMS dosage optimization, the BPA removal efficiency showed a distinct increase from 2.1% to 100% when the PMS concentration increased from 0 to 500 ppm. But when the PMS concentration was over 200 ppm, 100% BPA could be degraded. Therefore, 200 ppm was used in the following experiments.
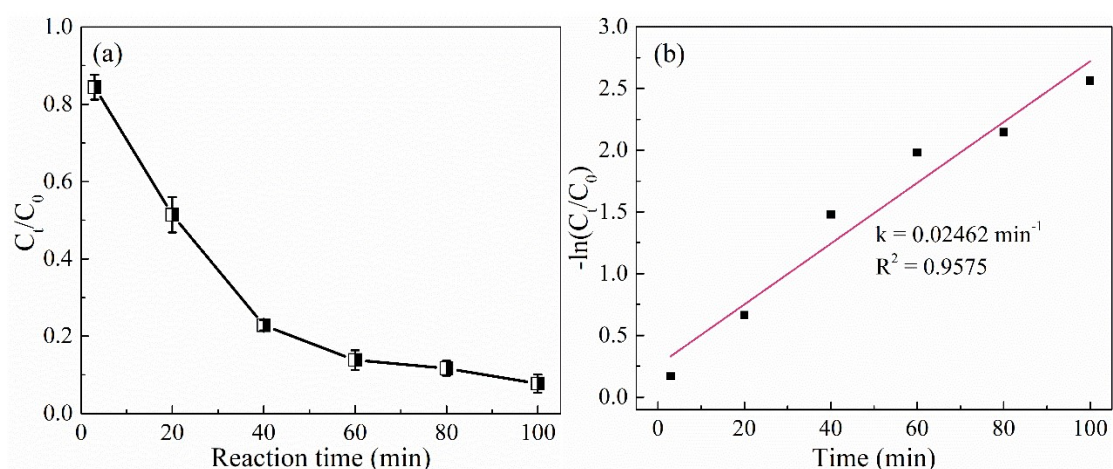

Figure S6. (a) BPA removal efficiency and (b) first-order kinetics of ZIF-67/GO-3 nanosheets in bulk solution. [catalyst] = 0.1 g L^{-1}, [BPA] = 5 mg L^{-1}, [PMS] = 200 ppm, and pH 10.4.
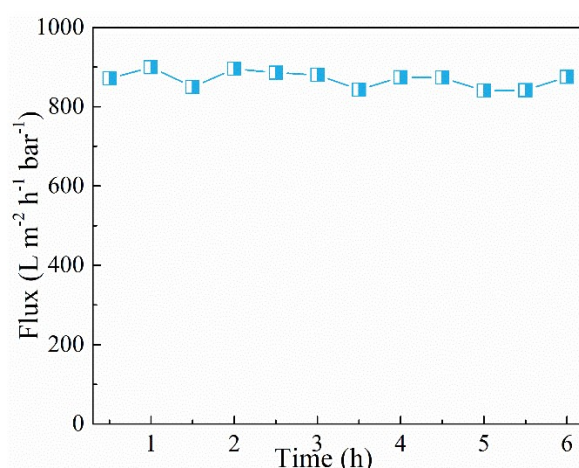

Figure S7. Stability test of flux with operation duration of the nanofluidic ZIF-67/GO-3 membrane of 1.4 μm in thickness.

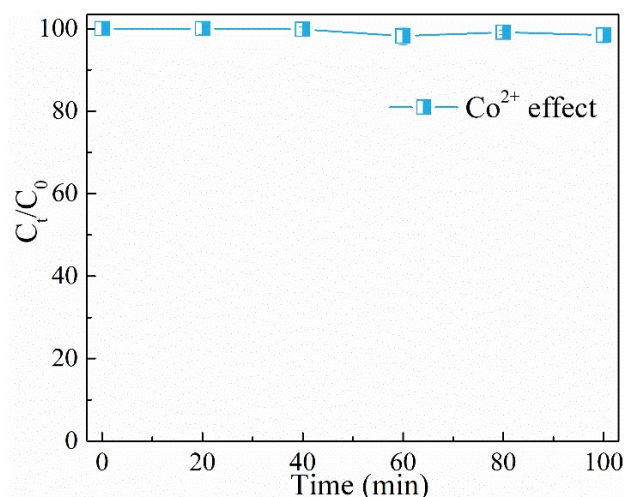**Figure S8.** Effect of the same amount of leached Co^{2+} (80 μg L^{-1}) on BPA degradation. Reaction conditions: [BPA] = 5 mg L^{-1}, [PMS] = 200 ppm, and pH 10.4.

For the consideration of sewage safety, the concentrations of K^+, SO_4^{2-} and 2-methylimidazole were also tested or calculated as follows:

PMS ($KHSO_5 \cdot 0.5KHSO_4 \cdot 0.5K_2SO_4$)

[PMS] = 200 ppm = 0.2 g L^{-1}

C_{PMS} = 0.2 g L^{-1} / 307.38 g mol^{-1} = 0.00065 mol L^{-1}

$[K^+]$ = 2.5 × C_{PMS} × 39 g mol^{-1} = 63.6 mg L^{-1}

[S] = 2 × C_{PMS} × 32 g mol^{-1} = 41.6 mg L^{-1}

$[SO_4^{2-}]$ = C_{PMS} × 96 g mol^{-1} = 62.4 mg L^{-1}

According to M. Arienzo et al[1] and Rpes.J.Bowell et al[2], these indicators are in line with the standards for sewage effluent.
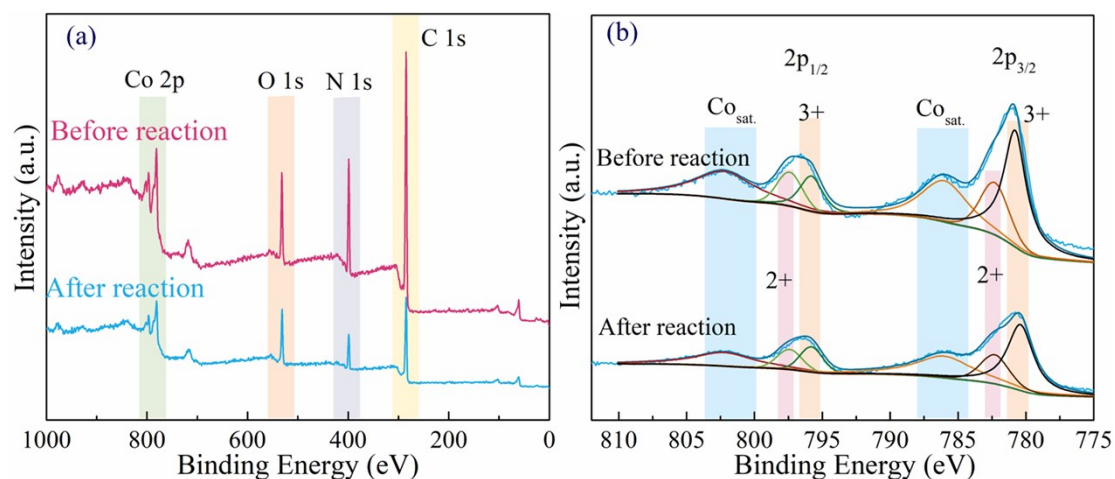

Figure S9. (a) XPS survey scan and (b) Co 2p spectra of ZIF-67/GO-3 before and after 6 h reaction.
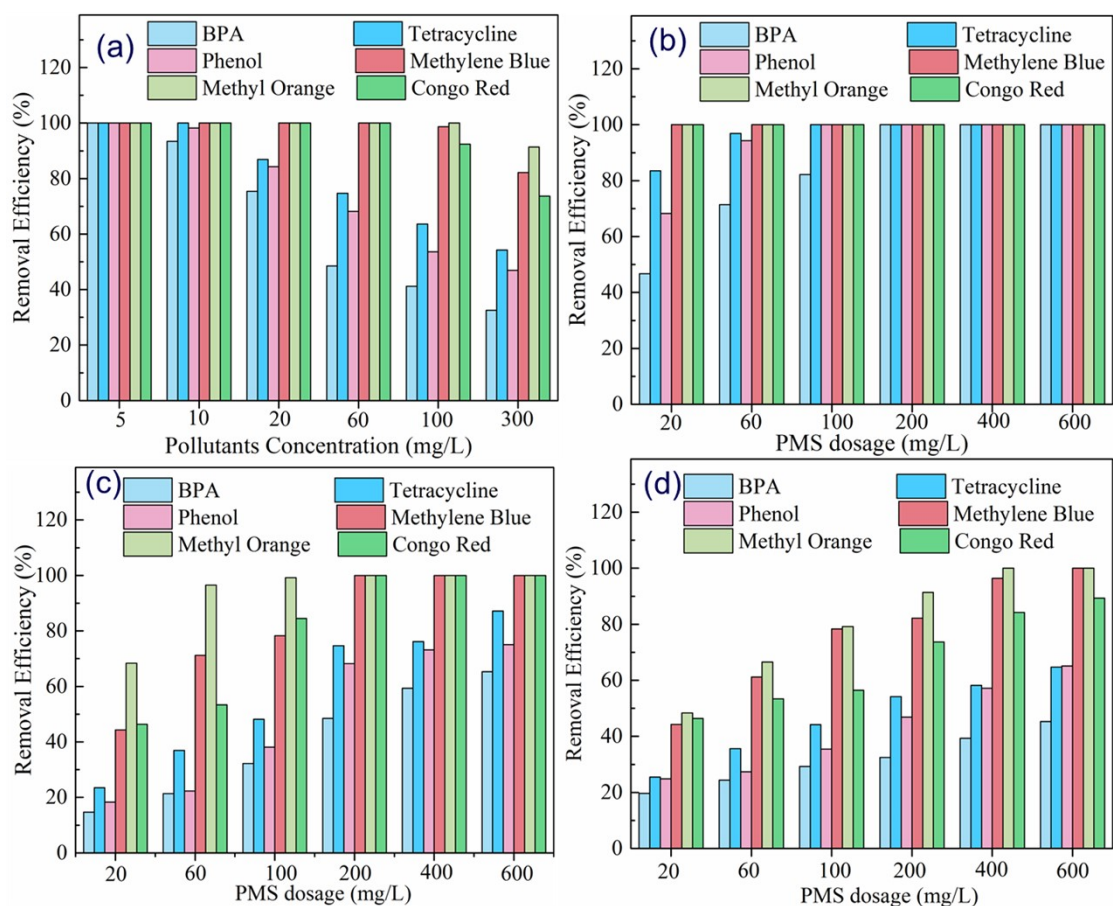
Figure S10. (a) The ZIF-67/GO-3 membrane/PMS system for treating wastewater with different BPA concentrations. (b-d) Comparison of pollutant removal efficiency of the ZIF-67/GO-3 membrane/PMS system as a function of PMS dosages and organic pollutant concentrations: 5 ppm (b), 60 ppm (c), and 300 ppm (d).
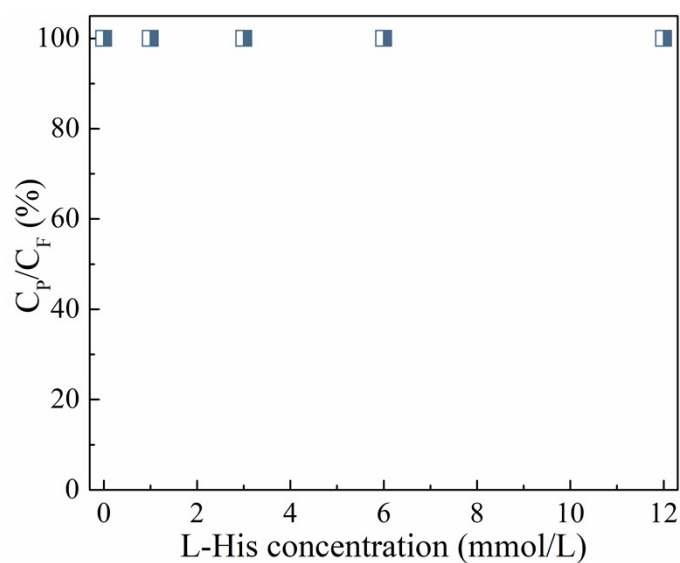

Figure S11. Quenching test of L-His for singlet oxygen $^1O_2$ with different concentrations. Reaction conditions: [BPA] = 5 mg L^{-1}, [PMS] = 200 ppm, and pH 10.4.

Singlet oxygen ($^1O_2$) attracted much attention in persulfate-based oxidation processes due to its wide pH tolerance and high selectivity toward electron-rich organics. With the addition of up to 12 mM L-His into the reaction system as a scavenger for $^1O_2$ [3], there was no variation in the BPA degradation efficiency. This result revealed that $^1O_2$ played a negligible role in the ZIF-67/GO-3 membrane/PMS system.
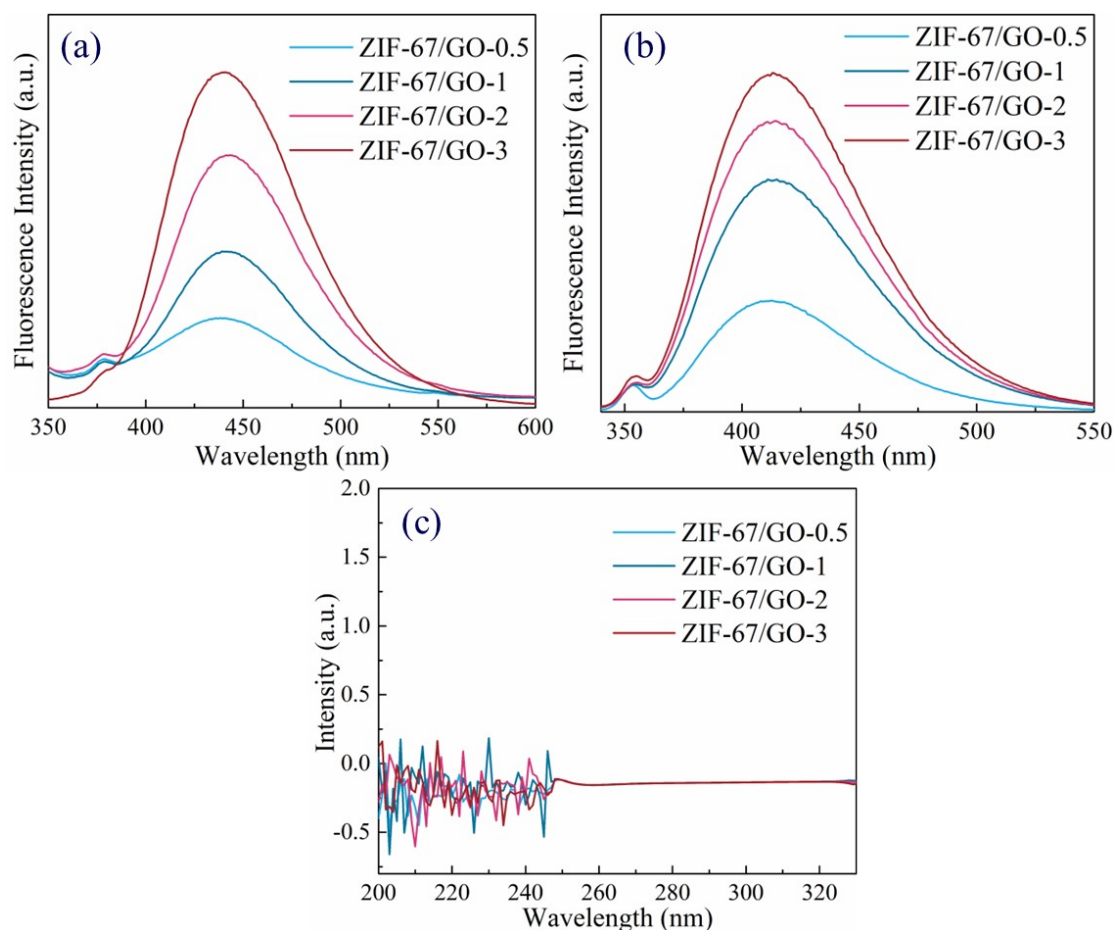

Figure S12. Fluorescence spectra of (a) •OH in terephthalic acid solution and (b) $SO_4^{·-}$ in benzoic acid solution. (c) UV spectra of $O_2^{·-}$ in benzoic acid solution.
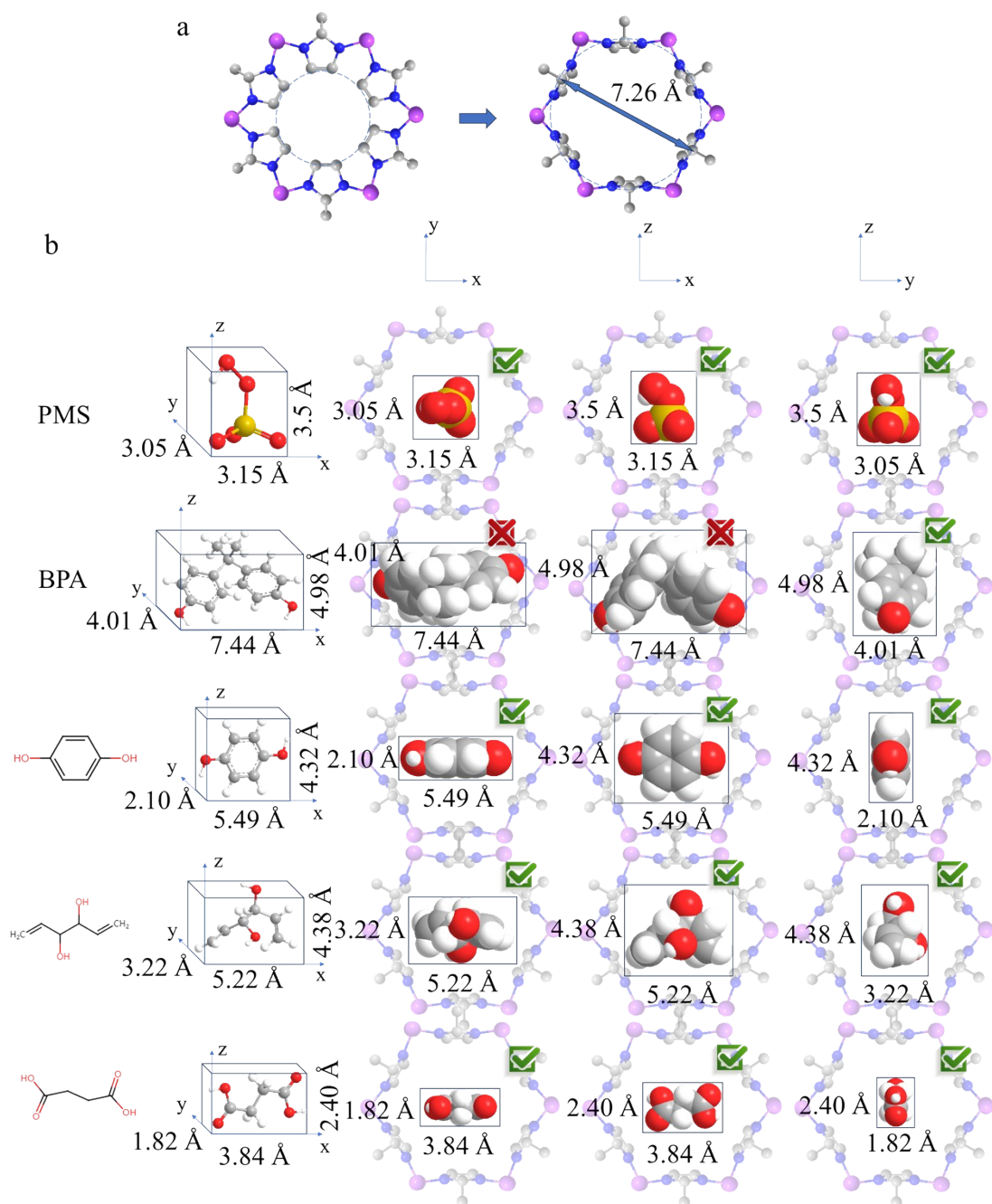
Figure S13. (a) Flexibility of ZIF-67 windows. (b) The molecular size of PMS, BPA, and byproducts in different dimensions. And maximum likelihood of entering the cavities of ZIF-67 in different angles for different molecules.
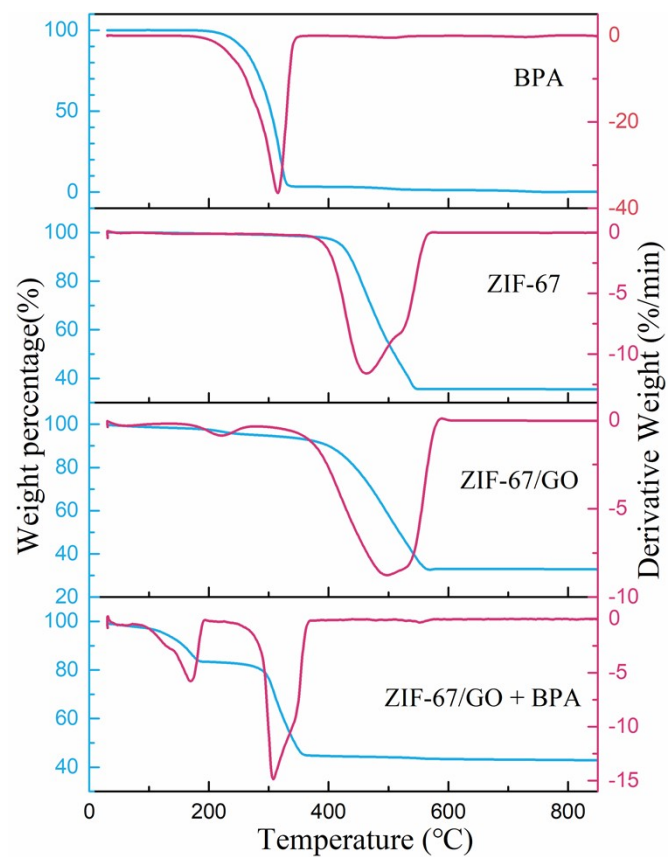
Figure S14. TG and DTG curves of BPA, ZIF-67, ZIF-67/GO, and ZIF-67/GO with absorbed BPA byproducts.

Table S1. Comparison of organic pollutant removal efficiency over different materials.

Materials	Water flux(L m^{-2} h^{-1} bar^{-1})	Pollutant (X, ppm)	Removal efficiency	Reaction time	Catalyst dosage/ Membrane thickness	PMS dosage (ppm)	k (min^{-1})	Ref
Co_3O_4@carbon	-	BPA, 40	99.0%	100 min	0.1 g L^{-1}	200	0.0431	4
V_O-Co_3O_4	-	BPA, 40	91.0%	100 min	0.2 g L^{-1}	200	0.0232	5
SACo-NGs	-	BPA, 22.8	100%	5 min	0.1 g L^{-1}	307	0.6	6
ZIF-8@67-C	-	BPA, 20	91.6%	15 s	0.1 g L^{-1}	100	14.4	7
Co@N-C	-	BPA, 50	100%	<10min	0.025 g L^{-1}	600	0.73	8
Co-TPML	-	BPA, 11.4	100%	5 min	0.2 g L^{-1}	614	<3	9
ZIF-67/GO nanosheet	-	BPA, 5	92.3%	100 min	0.1 g L^{-1}	200	0.0246	This work
$CuCo_2O_4$-CM membrane	822.5	BPA, 30	92.1%	33 ms	~15 μm	614	0.215	10
NFZ-5 membrane	127	BPA, 10	100%	40 min	0.3 μm	307	0.11	11
Co-BNNS membrane	750	Ranitidine, 5	99.13%	80 ms	0.3 μm	50	7866	12
ce-MoS_2 membrane	154	BPA, 2	>90%	60.4 ms	0.4 μm	50	0.65	13
MOF-d $Co_{1.75}Fe_{1.25}O_4$ membrane	200	BPA, 10	100%	1 min	-	153	0.11	14
ZIF-67/GO membrane	875	BPA, 5	100%	7.0 ms	1.38 μm	200	39000	This work
ZIF-67/GO membrane	941	Tetracycline, 5	100%	6.5 ms	1.38 μm	200	60000	This work
ZIF-67/GO membrane	862	Phenol, 5	100%	7.1 ms	1.38 μm	200	51600	This work
ZIF-67/GO membrane	828	Methylene blue, 5	100%	7.4 ms	1.38 μm	200	-	This work
ZIF-67/GO membrane	738	Methyl orange, 5	100%	8.3 ms	1.38 μm	200	-	This work
ZIF-67/GO membrane	901	Congo red, 5	100%	6.8 ms	1.38 μm	200	-	This work

Table S2. Kinetics (ms^{-1}) comparison of different pollutants dosages removal efficiency over ZIF-67/GO membrane.
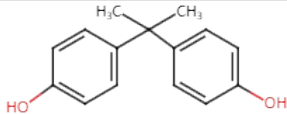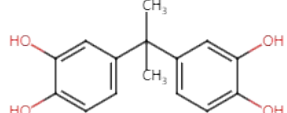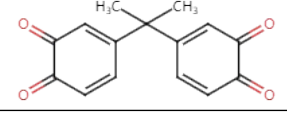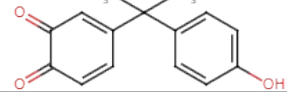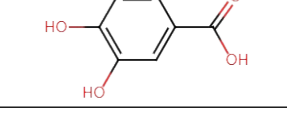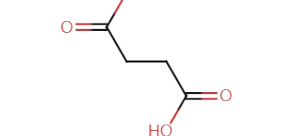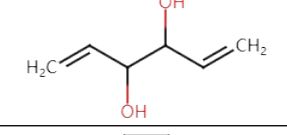
Pollutants Concentration	BPA	Tetracycline	Phenol	Methylene blue	Methyl orange	Congo red
5 ppm	39000	60000	51600	-	-	-
60 ppm	48600	90600	72600	93600	366600	124800
300 ppm	18000	36600	37800	139200	129600	78600

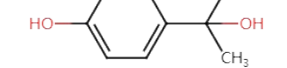Higher kinetics values could be achieved under higher pollutant dosages, which could develop competitiveness compared to other published literature (Table S1). From the authors' points of view, higher PMS catalyst dosages are needed if the pollutant dosages increase. These high concentrations might also raise the concern of secondary pollution or high running costs. Therefore, 5 ppm BPA and 200 ppm PMS are still chosen for the subsequent studies.

Table S3. XPS spectra of ZIF-67/GO-3 membrane before and after the reaction.

Element	Bond type	E/eV	at%	Peak area	FWHM	E/eV	at%	Peak area	FWHM
			Before reaction				After reaction		
O 1s			16.02				14.50		
C 1s			65.91				67.07		
N 1s			14.06				14.62		
Co 2p			4.01				3.81		
	≡Co(II)	781.1	39.63	82893.3	2.93	780.86	33.42	44107.6	2.98
		785.8	23.91	49985.4	3.91	785.45	26.89	35471.5	6.41
Co 2p		802.4	13.87	28943.8	5.40	802.22	14.27	18786.4	6.04
	≡Co(III)	775.3	7.85	16426.6	6.40	776.48	10.07	13299.4	10.67
		796.7	14.74	30791.2	2.69	796.5	15.35	20220.0	2.86

Table S4. Identification of intermediates by LC-MS during the BPA degradation process.

Name	Molecular Formula	Ion Mode	MS (m/z)		Structure
			Experiment.	Theory.	
Bisphenol A	$C_{15}H_{16}O_2$	Negative	227.1	228.3	
4,4`-Propane-2,2-diyldibenzene-1,2-diol	$C_{15}H_{16}O_4$	Positive	259.1	260.1	
4,4`-(2,2-Propanediyl)bis(1,2-benzoquinone)	$C_{15}H_{12}O_4$	Negative	255.2	256.3	
4,5-Bisphenol-o-quinone	$C_{15}H_{14}O_3$	Positive	241.2	242.3	
Protocatechuic acid	$C_7H_6O_4$	Positive	152.9	154	
4-(2-Hydroxy-2-propyl)phenol	$C_9H_{12}O_2$	Positive	150.9	152.2	
Succinic acid	$C_4H_6O_4$	Negative	117.2	118.1	
1,5-Hexadiene-3,4-diol	$C_6H_{10}O_2$	Positive	113.0	114.1	
Hydroquinone	$C_6H_6O_2$	Negative	109.2	110.1	

References:

1. M. Arienzo, E. W. Christen, W. Quayle and A. Kumar, *J. Hazard. Mater.*, 2009, **164**, 415-422.
2. R. J. Bowell. *Proc. Inter. Mine Water*, 2004. **2**. 75-91.
3. Z. Feng, Q. Tian, Q. Yang, Y. Zhou, H. Zhao and G. Zhao, *Appl. Catal., B*, 2021, **286**, 119908.
4. J. Hu, B. Qian, X. Zeng, Y. Qi, Y. Liu, L. Zhang and X. Zhang, *J. Mater. Chem. A*, 2021, **9**, 16489-16499.
5. J. Hu, X. Zeng, G. Wang, B. Qian, Y. Liu, X. Hu, B. He, L. Zhang and X. Zhang, *Chem. Eng. J.*, 2020, **400**, 125869.
6. H. Zhang, L. Lyu, Q. Fang, C. Hu, S. Zhan and T. Li, *Appl. Catal., B*, 2021, **286**, 119912.
7. C. Zhu, Y. Nie, S. Zhao, Z. Fan, F. Liu and A. Li, *Appl. Catal., B*, 2022, **305**, 121057.
8. L. Wu, B. Li, Y. Li, X. Fan, F. Zhang, G. Zhang, Q. Xia and W. Peng, *ACS Catal.*, 2021, **11**, 5532-5543.
9. C. Chu, J. Yang, X. Zhou, D. Huang, H. Qi, S. Weon, J. Li, M. Elimelech, A. Wang and J. H. Kim, *Environ. Sci.Technol.*, 2021, **55**, 1242-1250.
10. Y. Huang, Y. Yang, Z. Guan, Q. Li and D. Xia, *J. Environ. Chem. Eng.*, 2023, **11**, 109500.
11. M. Li, S. You, X. Duan and Y. Liu, *Appl. Catal., B*, 2022, **312**, 121419.
12. M. B. Asif, S. Zhang, L. Qiu and Z. Zhang, *Chem. Cataly.*, 2022, **2**, 550-562.
13. Y. Chen, G. Zhang, H. Liu and J. Qu, *Angew. Chem. Int. Ed.*, 2019, **58**, 8134-8138.
14. W. Qu, H. Wen, X. Qu, Y. Guo, L. Hu, W. Liu, S. Tian, C. He and D. Shu, *Chemosphere*, 2022, **303**, 135301.